



OPEN Experimental study on recycling rubber to increase the impact resistance of cement mortar

Tao Ran^{1,2}, Jianyong Pang¹✉ & Di Wu¹

The COVID-19 pandemic has led to a surge in medical waste generation, posing hazards to both the environment and global health. The impacts of the COVID-19 pandemic's medical waste hazard may persist long after the pandemic itself subsides. Improper disposal of medical waste can contaminate environment, posing risks to ecosystems and public health. Discarded medical rubber gloves, for example, can become a source of infection, improper disposal of these gloves can escalate the spread of infectious diseases and increase the risk of transmission of the virus to the general public. This study proposes an innovative and sustainable method to reinforce cement mortar by adding recycled glove rubber as an additive to cement mortar to increase its resistance to impact loads. This study conducted uniaxial compression tests, separating hopkinson pressure bar (SHPB) experiments and SEM observations to evaluate the quasi-static compressive strength and dynamic stress of recycled rubber fiber mortar (RRFM) with varying recycled rubber fiber (RRF) contents (0, 1%, 2%, 3%). Strain curves, dynamic increase factor (DIF), energy absorption rules, failure modes, and microstructure of RRFM mixtures. The experimental results demonstrate that with the addition of RRF, the dynamic stress-strain curve flattens and the peak strain gradually increases. The RRFM sample shows stronger toughness. In comparison to regular cement mortar (NM), RRFM has a higher DIF and specific absorbed energy, a faster increase in dynamic compressive strength, and the ability to absorb more energy per unit volume. Under the same impact load, RRFM has fewer and smaller cracks than NM. Scanning electron microscopy (SEM) testing also observed that RRF formed a strong connection pattern with the cement mortar matrix.

Keywords Cement mortar, Recycled rubber, Separating hopkinson pressure bar, Waste management

During the COVID-19 epidemic, a huge number of medical facilities were utilized to control the outbreak's spread, and the treatment of medical waste after usage is a lengthy process¹⁻⁵. The large amount of medical waste remaining includes disposable protective equipment, such as masks^{6,7}, gloves^{8,9}, protective clothing^{10,11}; medical devices and equipment, including syringes¹, catheters¹², needles¹³, pharmaceutical packaging¹⁴; medical waste and waste liquid containers; medical waste garbage bags and packaging¹⁵, and infectious waste¹⁶.

Large amounts of medical waste can generate a variety of challenges. These problems include environmental pollution, because medical waste that is not properly treated may release harmful substances¹⁷⁻²⁰, threatening soil, water, and air quality, harming ecosystems and human health; public health risks, considering discarded medical waste may contain infectious pathogens, which become vectors for spreading diseases and increase public health risks^{21,22}; waste of resources, due to large-scale medical waste leads to waste of raw materials and energy. Medical waste could become a source of disease transmission, increasing biosecurity issues^{23,24}. As a consequence, proper disposal of any residual medical waste is critical, and appropriate steps must be implemented to reduce any environmental and public health risks. The disposal of discarded gloves is a major priority among all types of medical waste, as gloves are the most prevalent medical items with which medical personnel come into touch. Each medical staff member uses them multiple times every day and has a high contactivity²⁵⁻²⁷. Proper disposal of discarded medical gloves is critical to minimizing the potential harm caused by medical waste to the environment and public health.

Concrete is quite important in today's environment. It is not only the primary material for infrastructure and residential construction, but it also plays an important role in water conservation projects, environmental protection, and other disciplines²⁸. Its strength, durability, and plasticity allow numerous projects to serve individual life and development demands consistently and reliably. At the same time, concrete actively

¹School of Civil Engineering and Architecture, Anhui University of Science and Technology, Huainan 232001, China.

²School of Computing, Macquarie University, Macquarie Park, NSW 2109, Australia. ✉email: jypang@aust.edu.cn

contributes to environmental protection through recycling and carbon capture^{29–31}. The common material used to make medical gloves is nitrile rubber, and rubber is often used as an admixture for concrete to improve its ductility, toughness, fatigue performance and durability^{32–34}. Qiao³⁵ has proven through experiments that adding modified rubber additives can significantly improve the compressive strength, tensile strength, chloride ion penetration resistance and energy absorption capacity of concrete. He³³ proved that modified rubber additives can significantly improve the compressive, bending, tensile and impact resistance properties of rubber concrete, and surface modification enhances the adhesion between rubber and cement. Liu³⁶ investigated the influence of rubber content on the softening of concrete after fracture by performing three-point bending tests on ordinary and rubber beams (10%, 20%, 30%). The results suggest that adding rubber prolongs crack propagation, improves concrete deformation, and reduces stress concentration. Rubber decreases the occurrence and extent of cracks while also increasing the time it takes for concrete to soften. Su³⁷ encouraged the recycling of used tires in cement-based materials by enhancing the flexural and compressive strengths of mortar and lowering shrinkage by incorporating recovered steel fibers and plastic-rubber composites. Kumar³⁸ replaced grade six rubber powder (0–30%) with a particle size of 0.6–2.36 mm for fine aggregate. In acid environment, rubber concrete has better flexibility and impact resistance than ordinary concrete. Chen³⁹ created rubber fine aggregates of various sizes, contents, and pretreatment procedures with compressive strengths ranging from 16.5 to 34.3 MPa, and used computed tomography and scanning electron microscopy to study their effect on the mesostructure of concrete.

At the same time, rubber concrete can withstand higher impact loads than ordinary concrete. Rubber concrete has exceptional flexibility and seismic resilience, allowing it to effectively absorb impact energy. Chen⁴⁰ investigated the effects of rubber replacement rate, particle size, and strain rate on the impact resistance of self-compacting concrete using split hopkinson pressure bars (SHPB). The results show that, as compared to regular self-compacting concrete, rubber self-compacting concrete has higher dynamic peak strains and stresses, and rubber particles ranging from 1 to 2 mm have higher strength. Feng⁴¹ investigated the dynamic compression performance and strain rate sensitivity of rubberized concrete with rubber contents of 0, 10%, 20%, 30%, 40%, and 50%, respectively. The dynamic increase factor (DIF) increases with increasing strain rate, and rubber concrete has higher toughness and smaller fragment size after testing than ordinary concrete.

To successfully transform medical waste, such as rubber gloves, into valuable resources, this study used the Separating Hopkinson Pressure Bar (SHPB) method to conduct dynamic impact studies on cement mortar containing varying quantities of recycled rubber fibers (RRF). Due to the limited volume of rubber gloves, crushing them proven to be a better option for enabling experimental study. The RRF was produced by cutting the rubber gloves. The volume fractions of RRF in the cement mortar were 0%, 1%, 2%, and 3%, respectively. The variations in the dynamic stress-strain curves of cement mortar under different RRF content were initially investigated. Subsequently, the relationships between dynamic compressive strength, dynamic strength enhancement coefficient, and specific energy absorption with RRF content and impact pressure were analyzed. Finally, the bonding performance of RRF with the cementitious matrix was observed through SEM analysis. This study contributes to expanding the strategies for handling residual medical waste post-pandemic, aiming to minimize potential hazards to the environment and public health to the greatest extent possible.

Materials and methods

Raw materials

The cementitious material utilized in this experiment is PO.42.5 ordinary Portland cement produced in Huainan, China, with its chemical composition provided in Table 1. Ordinary river sand with a fineness modulus of 2.7 and an apparent density of 2700 kg/m³ was used as fine aggregate. Laboratory tap water was employed as the mixing water. To prevent viral transmission, disposable rubber gloves used in the experiment were brand new and unused. After being cut, the rubber gloves were incorporated into the cement mortar, and the specific physical properties of the recycled rubber fibers (RRF) are presented in Table 2.

Mix ratio, testing methods

The recycled rubber fibers (RRF) obtained from disposable rubber gloves were added as additives into the cement mortar, dividing the experiment into two groups: the ordinary mortar (NM group) as the control group and the recycled rubber fiber mortar (RRFM group) as the experimental group. RRF is added as an additive to cement mortar materials, and the concentrations added are 1%, 2% and 3% according to the volume parameters, respectively, recorded as RRFM-10, RRFM-20 and RRFM-30. Although rubber materials have a reinforcing

Composition content (%)	Cement
SiO ₂	22.60
Al ₂ O ₃	5.03
Fe ₂ O ₃	4.38
CaO	63.11
MgO	1.46
SO ₃	2.24
Loss on ignition	1.18

Table 1. The chemical compositions of cement.

Fiber properties	PSF
Specific gravity	1.26
Tensile strength (MPa)	2.73
Tensile strength at break (MPa)	2.71
Rupture force (N)	4.15
Elongation at break (%)	103.55
Water absorption	14%
Aspect ratio	1:3

Table 2. Properties of Recycled Rubber Fiber (RRF)⁴³.

Group number	Cement (kg)	Sand (kg)	Water (kg)	RRF (%by volume)	Static compressive strength (MPa)
NM	480	337	183	0	31
RRFM-10	480	337	183	1	27
RRFM-20	480	337	183	2	22
RRFM-30	480	337	183	3	16

Table 3. Mixing proportions of the experiment(kg/m³).

effect, their main function in many applications is to improve the physical properties and environmental effects of cement materials, rather than simply enhancing the strength of concrete. Therefore, RRF is described as an additive here. The mixing ratios of each group are detailed in Table 3.

The dimensions of the specimens for uniaxial compressive strength tests were $\phi 50\text{mm} \times 100\text{ mm}$, with three parallel samples prepared for each group, and the results were averaged. Dynamic testing specimens were sized $\phi 50\text{mm} \times 25\text{ mm}$, with three parallel specimens made for each group to facilitate the selection of optimal test results. All specimens were cured for 28 days in an environment with a temperature of $20 \pm 2\text{ }^\circ\text{C}$ and relative humidity of 95%. To maintain dry conditions, all samples were dried in an oven at $85\text{ }^\circ\text{C}$ for 24 h before the start of the experiment.

The testing apparatus comprised an RDL-200 electro-hydraulic servo testing machine (Fig. 1) and a Separating Hopkinson Pressure Bar (SHPB) device (Fig. 2). Uniaxial compressive strength tests were conducted with a displacement loading rate of 1 mm/min. Impact air pressures of 0.3, 0.4, and 0.5 MPa were applied for SHPB experiments. Prior to initiating the SHPB experiments, Vaseline was applied to the end faces of the samples in contact with the bars to reduce friction and ensure uniform distribution of internal stresses along the sample direction. The preparation of specimens and the experimental procedure are illustrated in Fig. 3.

Results and discussion

Stress balance analysis

Figure 4 depicts the changes in projected stress, incident stress, reflected stress, and the sum of incident and reflected stress across impact time. It can be seen from the figure that the sum of the incident wave and reflected wave of the specimen almost coincides with the stress curve, indicating that the test reaches a stress equilibrium state without considering the time lag, and the dynamic strength of the cement mortar is credible at this time.

At this time, dynamic resistance strain gauges are employed to capture waveform data, and matching formulas are used to calculate the strain rate $\dot{\varepsilon}_t(t)$, strain $\varepsilon_t(t)$ and dynamic stress $\sigma(t)$ of the specimen. $\dot{\varepsilon}_t(t)$, $\varepsilon_t(t)$ and $\sigma(t)$ are calculated using the formula (1). When the stress reaches equilibrium, $\varepsilon_t(t) = \varepsilon_i(t) + \varepsilon_r(t)$, the formula is further simplified to formula (2). This formula is the balanced two-wave method. The calculation is simple and the accuracy meets the experimental requirements. This method is used in the calculation method of this article.

$$\begin{cases} \dot{\varepsilon}_t(t) = \frac{c_0}{l_s} [\varepsilon_i(t) - \varepsilon_t(t) + \varepsilon_r(t)] \\ \varepsilon_t(t) = \frac{c_0}{l_s} \int_0^t [\varepsilon_i(t) - \varepsilon_t(t) + \varepsilon_r(t)] dt \\ \sigma(t) = \frac{AE}{2A_s} [\varepsilon_i(t) + \varepsilon_t(t) + \varepsilon_r(t)] \\ \varepsilon_t(t) = \varepsilon_i(t) + \varepsilon_r(t) \end{cases} \quad (1)$$



Fig. 1. RDL-200 electro-hydraulic servo testing machine.

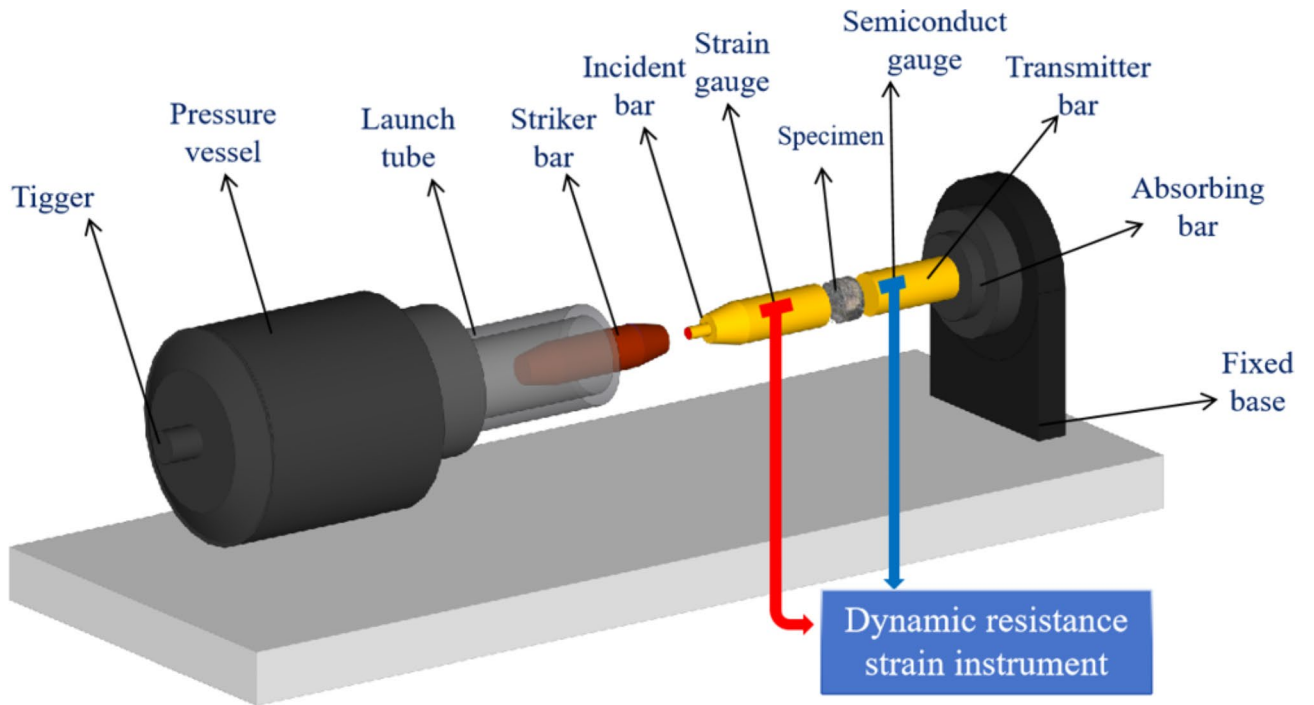


Fig. 2. Schematic diagram of the Separating Hopkinson pressure bar (SHPB)⁴².



Fig. 3. Experimental procedure diagram.

$$\begin{cases} \varepsilon^1(t) = -\frac{2c_0}{l_s} \varepsilon_r(t) \\ \varepsilon(t) = -\frac{2c_0}{l_s} \int_0^t \varepsilon_r(t) dt \\ \sigma(t) = \frac{AE}{A_s} \varepsilon_t(t) \end{cases} \quad (2)$$

In the formula: $\varepsilon_i(t)$, $\varepsilon_r(t)$, $\varepsilon_t(t)$, are the incident strain, reflected strain and transmitted strain at time t, l_s is the test strain thickness of the specimen, C_0 and E represent the longitudinal wave velocity and elastic modulus of the pressure bar, respectively. A, A_s represent the cross-sectional areas of the pressure bar and the specimen.

The static stress-strain curve

The stress-strain response curves of each group of cement mortar samples are given in Fig. 5. By observing the experimental results, it can be found that with the increase of RRF content, the peak stress of the cement mortar specimens began to decrease, and compared with the control group, it decreased by 4 MPa, 9 MPa and 15 MPa respectively. This proves that the addition of RRF has a weakening effect on the peak strength of cement mortar specimens, and the weakening effect is more obvious with the increase of content. However, it is also observed that with the increase of RRF content, the peak strain also increases accordingly, and the two are positively

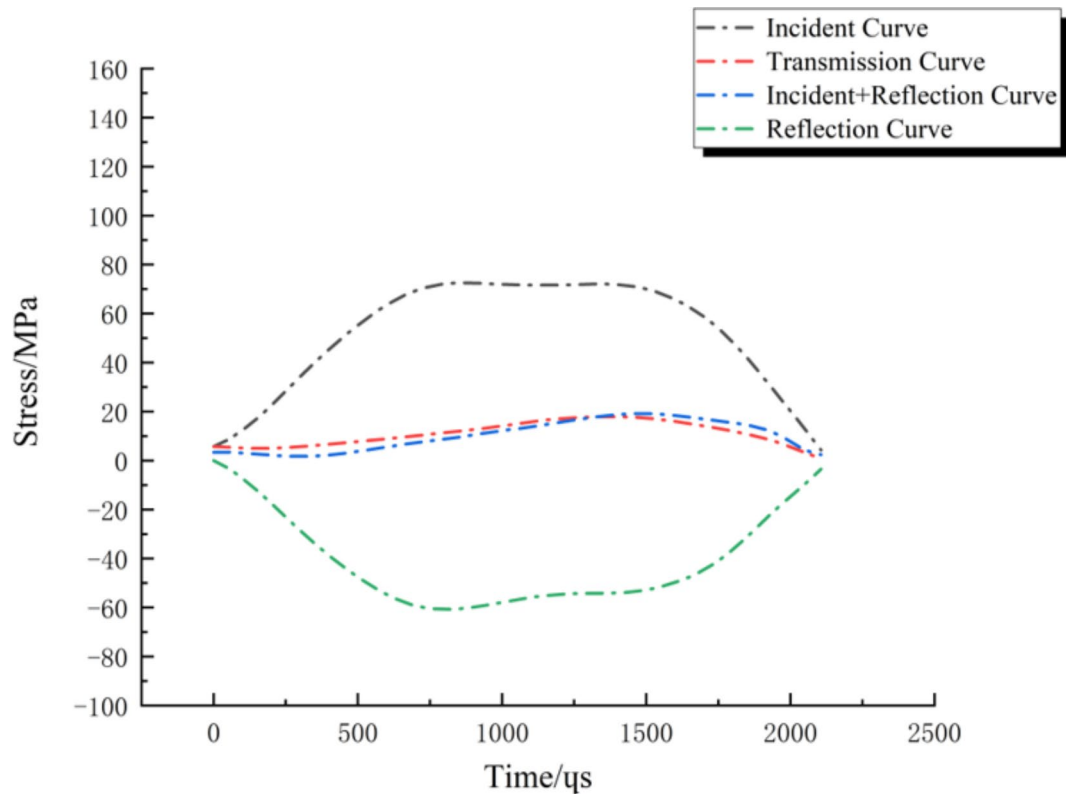


Fig. 4. Dynamic stress equilibrium.

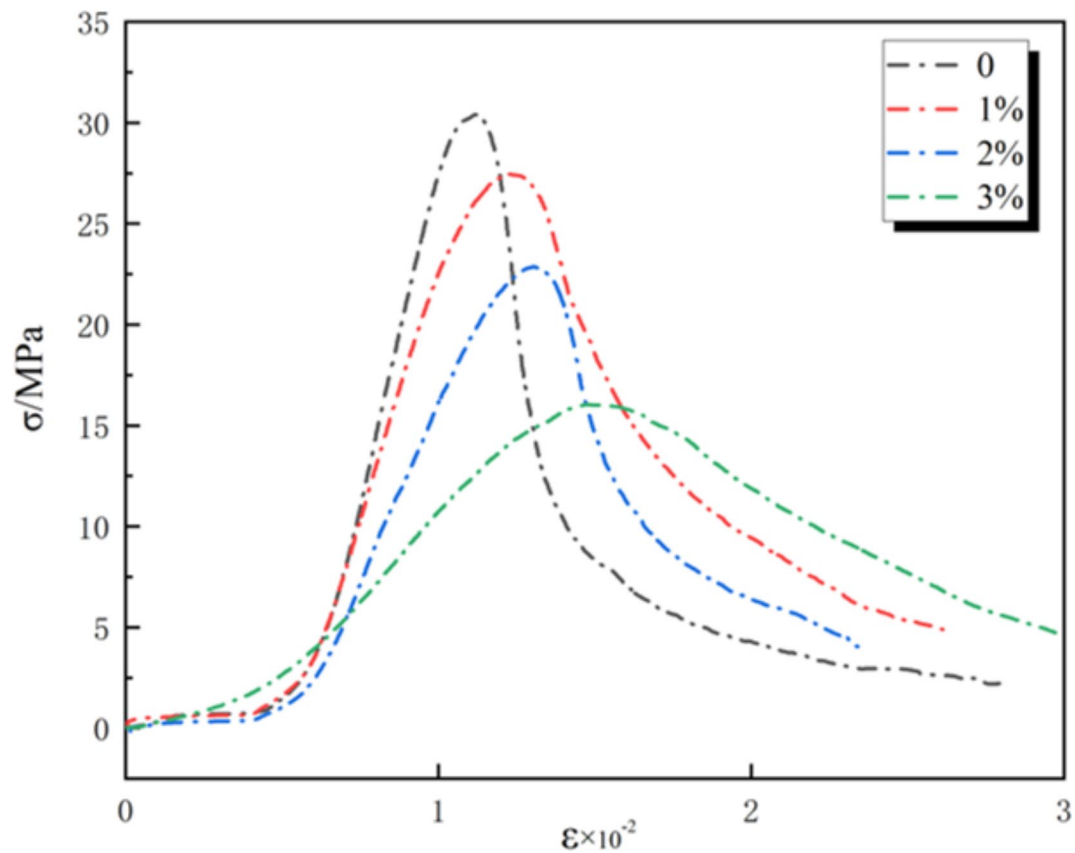


Fig. 5. Static stress-strain curves of specimens.

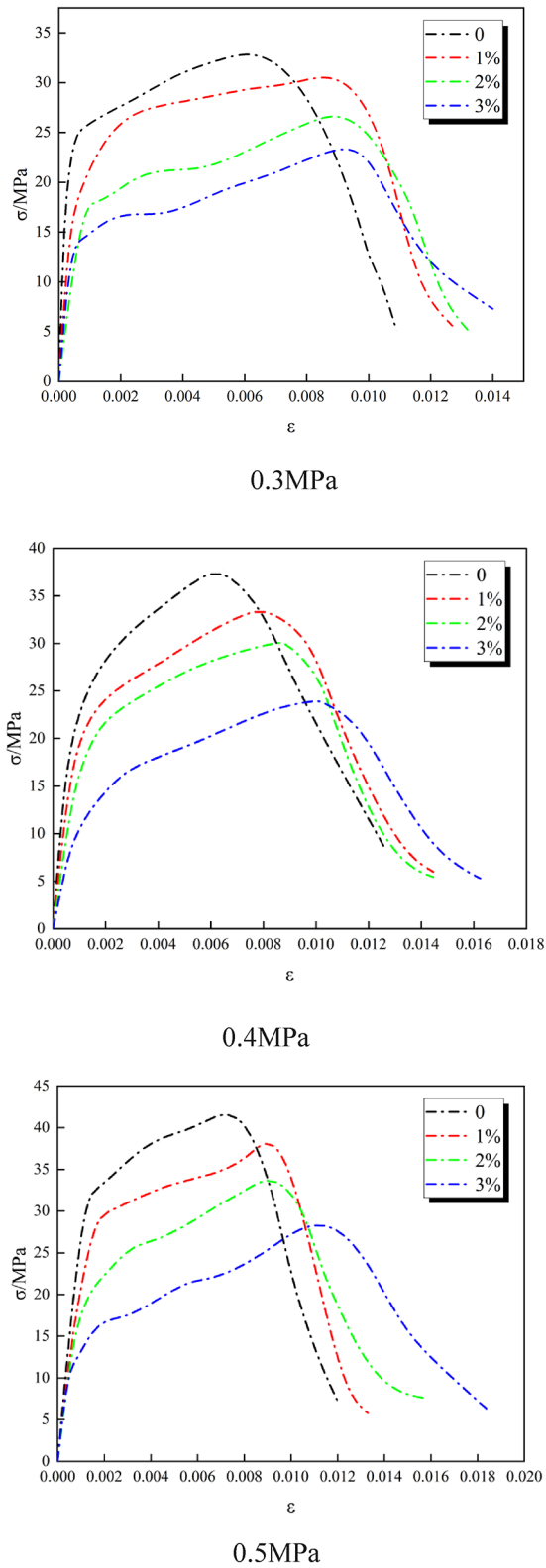


Fig. 6. Dynamic stress-strain curves of specimens with impact air pressures of 0.3 MPa, 0.4 MPa, and 0.5 MPa.

correlated. Thanks to the elasticity of RRF, cement mortar specimens can produce greater deformation when subjected to external loads, and the corresponding peak strain is also increased.

The dynamic stress-strain curve

The dynamic stress-strain curve accurately depicts the mechanical behavior changes of cement mortar under impact loading. Using the “Equilibrium Two-Wave Method,” dynamic stress-strain curves for various groups of specimens with variable rubber contents and impact pressures were generated. Figure 6 shows the dynamic stress-strain curves of cement mortar specimens with varying rubber contents at impact pressures of 0.3 MPa, 0.4 MPa, and 0.5 MPa, respectively. From figure, it can be observed that the dynamic peak strength of the RRFM group is consistently higher than the static compressive strength. Under the same impact pressure, as the RRF content increases, the dynamic stress-strain curves of each group gradually tend to flatten, and the peak strength under dynamic impact decreases gradually. However, both the peak strain and ultimate strain gradually increase, indicating a ductile failure mode of the RRF specimens. When the impact pressure is 0.4 MPa, with the increase in RRF content, the peak stress gradually increases to 37.82 MPa, 33.75 MPa, 30 MPa, and 24 MPa, while the peak strain increases to 0.0065, 0.0081, 0.0089, and 0.0102, respectively. The stress-strain curve fluctuation of RRFM under dynamic impact can be broadly classified as the following stages: Initially, the stress-strain curve rises rapidly, owing mostly to the compaction of internal cavities in the specimen. The stress-strain curve then gradually rises, indicating the elastic deformation stage of RRFM, until it achieves peak stress. Beyond the peak stress, strain increases while stress steadily drops until the specimen fails, demonstrating ductile qualities when compared to normal cement mortar.

Dynamic compressive strength

The relationship between dynamic compressive strength of specimens and RRF content under different impact pressures is illustrated in Fig. 7. As the RRF content increases, the dynamic compressive strength of each group gradually decreases. With the amplification of impact pressure, the dynamic compressive strength of the same specimens gradually increases. Under identical conditions, specimens containing recycled rubber exhibit lower dynamic compressive strength compared to ordinary concrete specimens, consistent with the conclusions of previous studies⁴⁴. The dynamic compressive strength of cement mortar specimens is influenced by the rubber content and impact pressure.

Dynamic peak strain

Figure 8 shows the curve of peak strain changing with rubber content under different impact pressures. By observing the graph, it can be seen that when the rubber content is the same, the peak strain will increase with increasing impact pressure, because the increase in impact pressure increases the strain rate of the specimen.

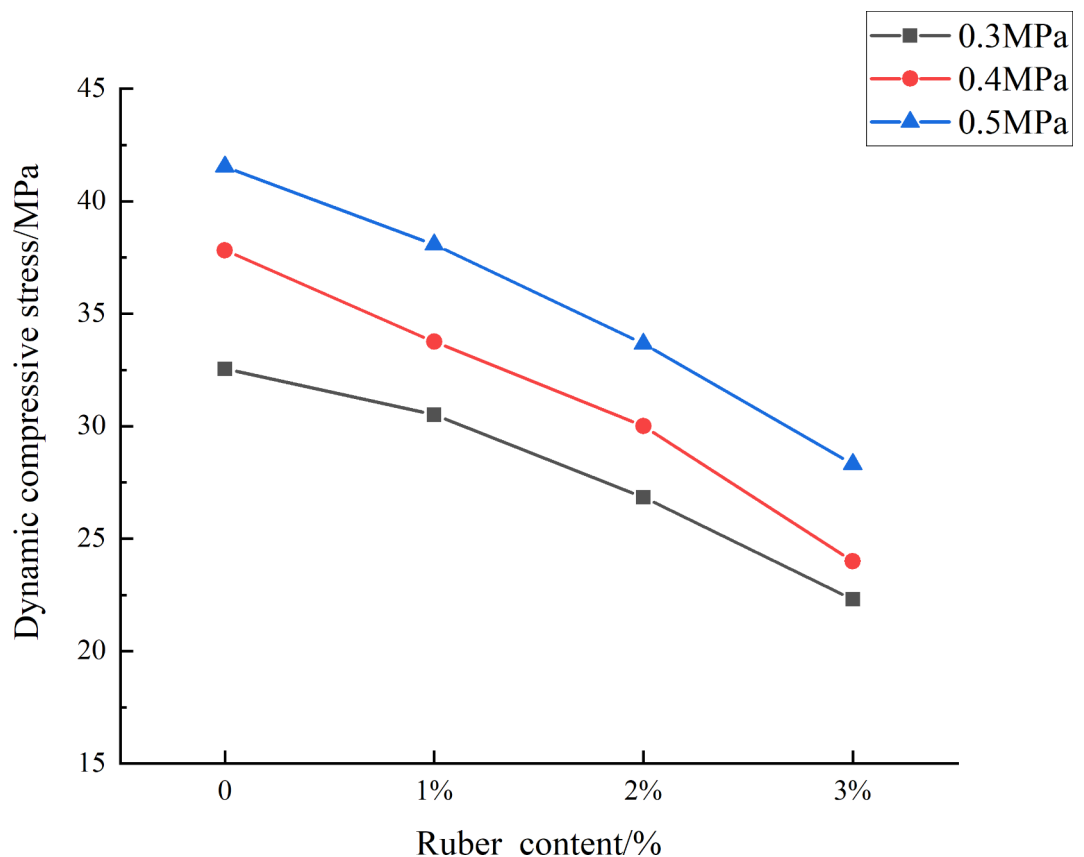


Fig. 7. The relationship between dynamic compressive strength and rubber content under different impact pressures.

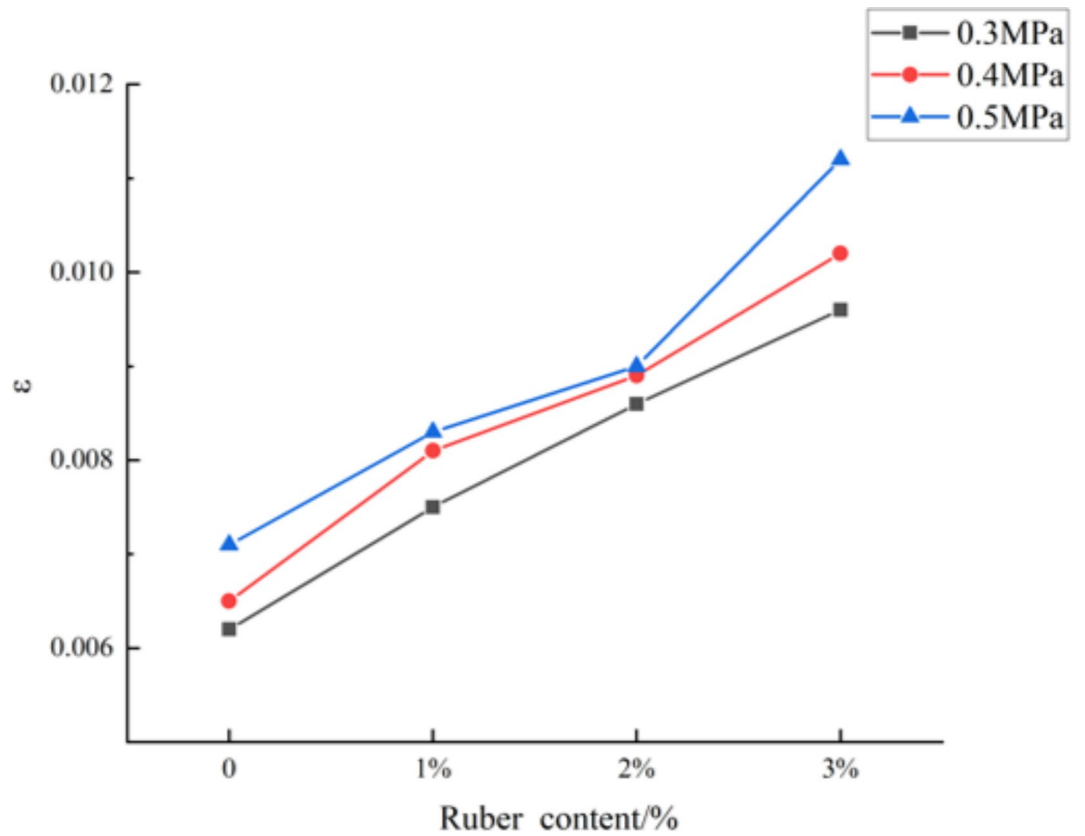


Fig. 8. The relationship between dynamic peak strain and rubber content under different impact pressures.

When the impact pressure remains unchanged, the addition of RRF also increases the peak strain of the cement mortar specimen, with a maximum increase of 57.8% when the impact pressure is 0.5 MPa. This is because the larger elasticity of RRF allows the cement mortar to produce a larger deformation, and the corresponding peak strain is also increased.

Dynamic increase factor (DIF)

The dynamic increase factor (DIF) is well recognized as a significant measure for assessing the strain rate effect: DIF equals the dynamic compressive strength divided by the static compressive strength. Figure 9 illustrates the relationship between DIF and rubber content as well as impact pressure.

The figure shows that the Dynamic Increase Factor (DIF) increases with increasing impact pressure and rubber content. This means that when the impact pressure and RRF content increase, consequently increases the ratio of the compressive strength of the specimen under dynamic versus static conditions. When the rubber content is 3% and the impact pressure is 0.5 MPa, the DIF reaches its maximum value, showing that the specimen’s compressive strength increase under dynamic conditions is maximized compared to static conditions. At this time, compared to the NM group, the enhancement rate reaches 32.1%. This pattern suggests that increasing the impact pressure and RRF content contributes to enhancing the compressive performance of the specimen under dynamic loading. The magnitude of DIF values is positively correlated with rubber content and impact pressure. When the impact pressure remains constant, the addition of rubber can enhance the DIF of cementitious materials.

Specific energy absorption

$$\begin{cases} W_i(t) = AEC \int_0^t \varepsilon_i^2(t) dt \\ W_r(t) = AEC \int_0^t \varepsilon_r^2(t) dt \\ W_t(t) = AEC \int_0^t \varepsilon_t^2(t) dt \end{cases} \quad (3)$$

$$W_s(t) = W_i(t) - W_r(t) - W_t(t) \quad (4)$$

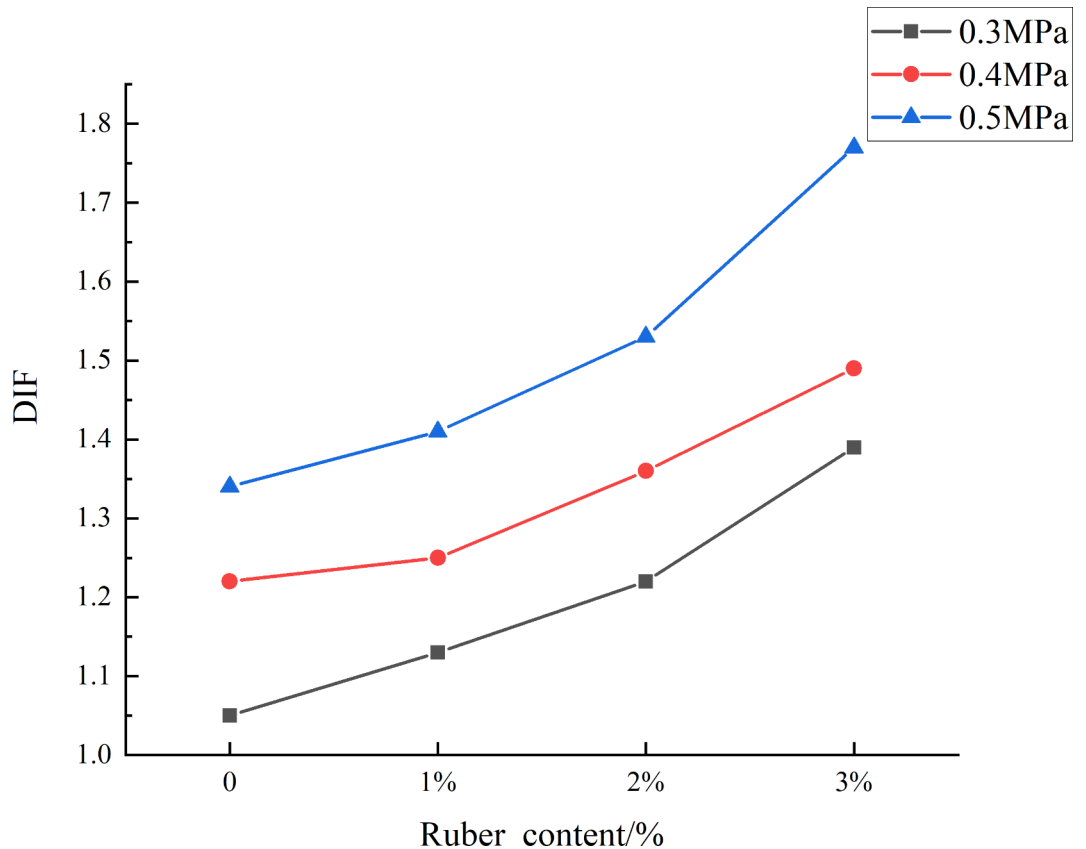


Fig. 9. The relationship between DIF and rubber content under different impact pressures.

$$\lambda = \frac{W_s}{V_s} \quad (5)$$

In the formula (3), (4): W_i represents the incident energy, W_t represents the transmitted energy, W_r represents the reflected energy, W_s represents the energy absorbed by the specimen during failure, A denotes the cross-sectional area of the specimen, E represents the elastic modulus of the pressure bar material, C_0 denotes the longitudinal wave velocity in the pressure bar, and $\varepsilon_i(t)$, $\varepsilon_r(t)$ and $\varepsilon_t(t)$ represent the incident strain, reflected strain, and transmitted strain at time t , respectively.

Additionally, the specific energy absorption per unit volume λ is introduced in formula (5), where V_s represents the volume of the specimen.

From Fig. 10, the relationship between specific energy absorption and impact pressure can be observed. As the impact pressure increases, the specific energy absorption of the same specimen continuously increases. When the rubber content is 20%, the specific energy absorption corresponding to 0.3 MPa, 0.4 MPa, and 0.5 MPa is 0.522, 0.68, and 0.9 respectively, showing an increasing trend. As the impact pressure increases, the velocity of the bullet hitting the incident bar increases, resulting in more kinetic energy possessed by the bullet. Consequently, the incident energy obtained by the incident bar after being hit by the bullet also increases with the increase in impact pressure. With the increase in incident energy, the remaining energy consumed by the specimen after reflection and transmission also increases accordingly. Consequently, the specimen absorbs more energy, and there is a positive correlation between specific energy absorption and impact pressure.

Figure 11 illustrates the relationship between rubber content and specific energy absorption. With the increase in RRF content, there is an overall trend of increased specific energy absorption. At 0.4 MPa pressure, compared to the control group specimens, RRFM-10 exhibited a 22% increase in energy absorption, RRFM-20 showed a 41% increase, and RRFM-30 demonstrated a 56% increase in energy absorption. The addition of rubber enhances the energy absorption capacity of RRFM specimens, and as the rubber content increases, the RRFM specimens also show an increasing trend in impact energy absorption. For rubber-cement composite materials, the inclusion of rubber can introduce a large number of weak planes and pores into the cement mortar matrix. When subjected to external impact loads, the compaction of pores can provide space for the deformation of rubber. During the compression deformation process of pores and rubber, energy from the external environment is dissipated, allowing RRFM to play a role in flexible energy absorption under impact loads.

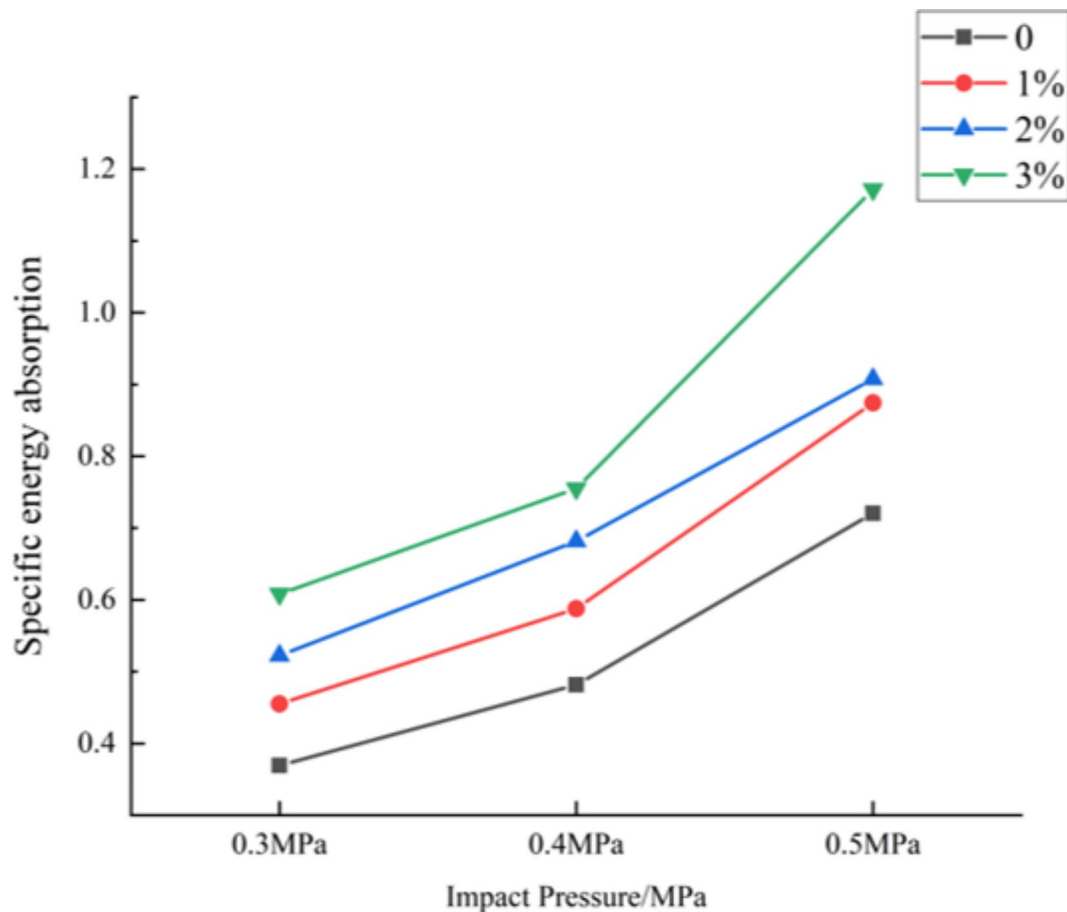


Fig. 10. The relationship between specific energy absorption and impact pressure.

Failure mode

Figure 12 presents typical images of the impact damage modes of cement mortar specimens with different RRF contents under various impact air pressures. Observing figure reveals significant changes in the final failure of specimens with increasing air pressure and RRF content. With the increase in air pressure, the failure mode of the NM group specimens gradually transitions from a blocky fragmentation state to a pulverized state. This indicates that the cement mortar without RRF exhibits brittle material characteristics, with weak resistance to impact deformation, and shows a pulverized pattern under higher air pressure. In contrast to the control group, specimens from the RRFM10, RRFM20, and RRFM30 groups show gradual collapse of the four sides of the specimens with increasing impact air pressure, accompanied by observed detachment of fragments. However, the specimens themselves remain relatively intact, and RRF can be observed connecting the fractured pieces on the failure surface, maintaining the integrity of the cement mortar specimens. This phenomenon suggests that the addition of a certain amount of RRF can resist the action of impact loads, resulting in a significant improvement compared to the complete brittle failure of ordinary cement mortar.

Through Fig. 12, it can be inferred that under the same air pressure, the ability of cement mortar to resist deformation gradually increases with the increase in RRF content. For instance, at an impact air pressure of 0.5 MPa, with RRF contents of 0%, 1%, 2%, and 3%, the failure modes of the specimens are pulverization, large blocks, partial fracture, and the appearance of obvious cracks, respectively. Thanks to the good crack-resistance effect of RRF, the failure morphology of the RRFM20 and RRFM30 groups is relatively complete, and the crack extension range is not large. It can be concluded that with the increase of RRF content, cement mortar gradually transitions to plastic failure, with greater energy absorption and enhanced ability to resist impact deformation, which provides experimental evidence for the practical application of high-content RRF in cement-based materials.

Scanning electron microscopy (SEM) image analysis

Figure 13 presents the SEM images of specimens from the RRF-20 group at different magnifications. From Fig. 13 ab, it can be observed that cement mortar particles adhere to the surface of the rubber, indicating good adhesion between RRF and the cement mortar matrix. The interface between RRF and the cementitious matrix forms a uniform and continuous interfacial transition zone (ITZ). (Fig. 13c,d,e) The formation of this transition zone facilitates a robust bond between RRF and the cementitious matrix. At higher magnifications, the rough surface texture of RRF is clearly visible (Fig. 13f), which also facilitates mechanical interlocking with the cement

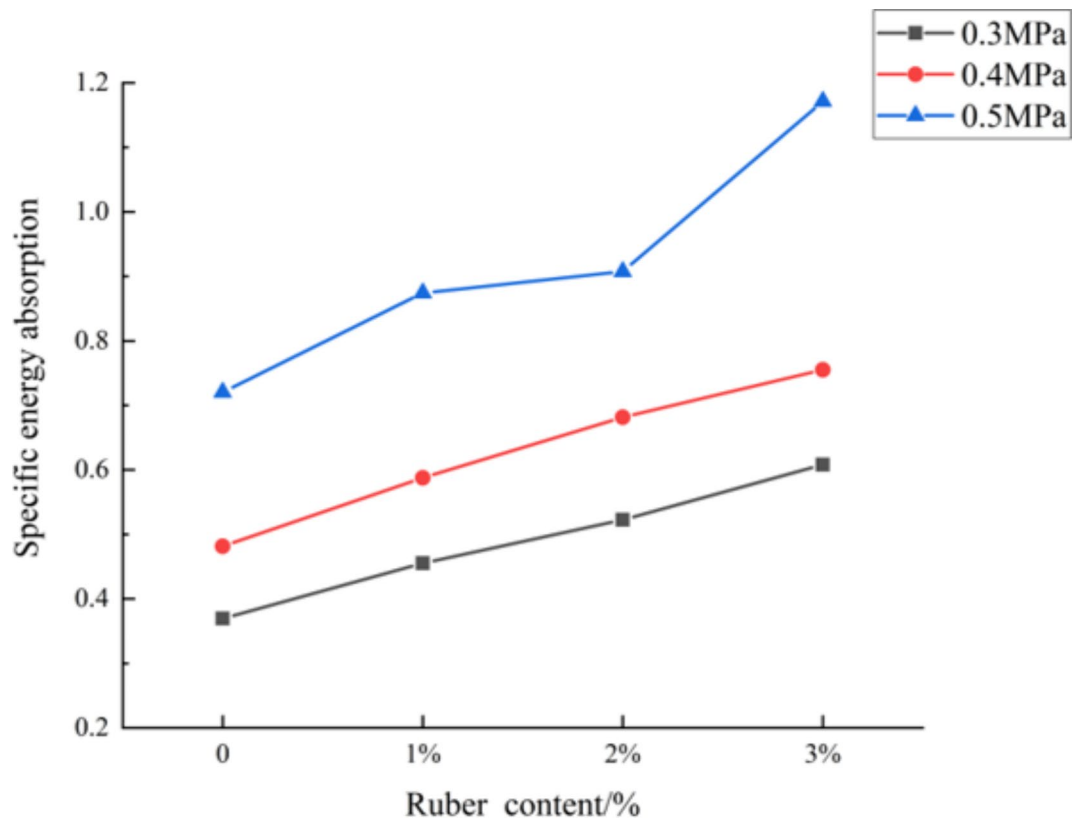


Fig. 11. The relationship between specific energy absorption and rubber content.

mortar matrix (Fig. 13g,h), thereby enhancing mechanical performance. Shen⁴⁵ made similar observations regarding the connection between polypropylene fibers and the cement matrix, which enhanced the anti-sliding properties and bond strength of the cement matrix. In addition, the randomly dispersed RRF in the cement mortar matrix cause cracks to deflect or bifurcate during propagation, increasing the complexity of the crack path, thereby dissipating more energy and limiting the large deformation of the cement mortar matrix when subjected to impact loads. At the same time, thanks to the better elasticity of RRF, the cement mortar obtains a larger allowable deformation, thereby increasing the energy dissipation when subjected to loads. Examination of the fracture surfaces provides compelling evidence for the contribution of RRF to the overall structural stability of the material. The effective connection of the RRF at the fracture interface can be observed in the failure mode diagrams, and this interconnected network acts as a reinforcement mechanism, holding the material together tightly and preventing catastrophic failure.

Conclusion

The Split Hopkinson Pressure Bar (SHPB) method was used to conduct a dynamic impact analysis of cement mortar containing varying percentages of recycled rubber fiber (RRF) in order to successfully convert medical waste, such as rubber gloves, into useful resources. By reducing potential risks to the environment and public health as much as feasible, this study helps to broaden the approaches for managing leftover medical waste after a pandemic. The following are the specific conclusions:

1. As RRF content increases, the RRFM dynamic stress-strain curve gradually flattens and the peak strain rises. It has higher toughness than the NM group because the stress declines slowly after reaching its peak.
2. The dynamic compressive strength is inversely proportional to the RRF content, but the dynamic strength growth factor (DIF) is positively linked to impact air pressure and RRF content. When the impact pressure is 0.5MPa, the DIF of RRFM-30 increases by 32.1% compared to the NM group.
3. As the RRF content increases, the specific absorbed energy of the specimen shows an overall increasing trend, which could be attributed to the flexible energy absorption effect of RRF when bearing impact loads.
4. The failure mode of the NM group exhibits brittle features. The addition of RRF mitigates the harmful effect of the impact load, and the breadth and number of cracks caused by the impact are greatly decreased. Comprehensive mechanical properties and failure modes, 0.2% RRF content is suitable.
5. Scanning electron microscopy (SEM) images demonstrate that RRF has good contact with the cement matrix, and the rough surface texture also helps to develop mechanical engagement with the matrix, which enhances mechanical characteristics.



Fig. 12. The failure modes of specimens under impact loading in each group.

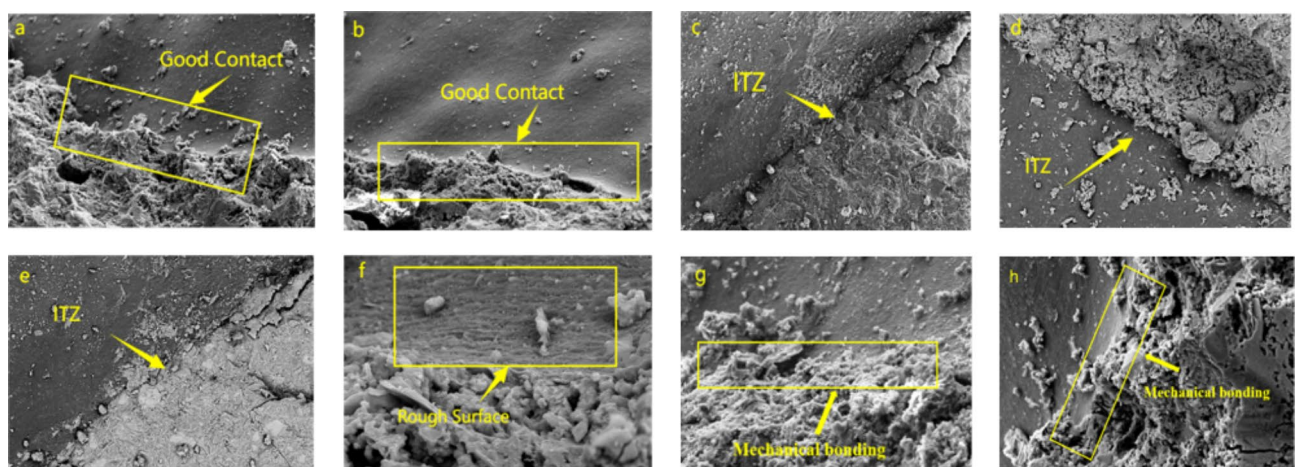


Fig. 13. Microstructure images of the RRF-20 group.

Data availability

The datasets used and/or analyzed during the current study available from the corresponding author on reasonable request.

Received: 17 April 2024; Accepted: 20 September 2024

Published online: 24 October 2024

References

- Karimi, H., Wassan, N., Ehsani, B., Tavakkoli-Moghaddam, R. & Ghodrathnama, A. Optimizing COVID-19 medical waste management using goal and robust possibilistic programming. *Eng. Appl. Artif. Intell.* **131**, 107838 (2024).
- Park, S. Assessing the impact of COVID-19 on waste generation: Focus on plastic, food, and medical wastes in South Korea. *Heliyon* **9**, e18881 (2023).
- Tang, J., Liu, X. & Wang, W. COVID-19 medical waste transportation risk evaluation integrating type-2 fuzzy total interpretive structural modeling and Bayesian network. *Expert Syst. Appl.* **213**, 118885 (2023).
- Cao, C., Xie, Y., Liu, Y., Liu, J. & Zhang, F. Two-phase COVID-19 medical waste transport optimisation considering sustainability and infection probability. *J. Clean. Prod.* **389**, 135985 (2023).
- Cao, C., Liu, J., Liu, Y., Wang, H. & Liu, M. Digital twin-driven robust bi-level optimisation model for COVID-19 medical waste location-transport under circular economy. *Comput. Ind. Eng.* **186**, 109107 (2023).
- Idowu, G. A. & Olonimoyo, E. A. How has COVID-19 medical face mask altered the dynamics of pollutants from incinerated wastes?. *J. Hazard. Mater. Adv.* **11**, 100351 (2023).
- Sangkham, S. Face mask and medical waste disposal during the novel COVID-19 pandemic in Asia. *Case Stud. Chem. Environ. Eng.* **2**, 100052 (2020).
- Ran, T., Pang, J., Liu, Y., Zou, J. & Cai, F. Improving concrete fatigue resistance with COVID-19 rubber gloves: An innovative sustainable approach. *Case Stud. Constr. Mater.* **18**, e01914 (2023).
- Kilmartin-Lynch, S., Roychand, R., Saberian, M., Li, J. & Zhang, G. Application of COVID-19 single-use shredded nitrile gloves in structural concrete: Case study from Australia. *Sci. Total Environ.* **812**, 151423 (2022).
- Ran, T., Pang, J. & Zou, J. An emerging solution for medical waste: Reuse of COVID-19 protective suit in concrete. 1–18 (2022).
- Zeng, F. et al. Advances and perspectives on the life-cycle impact assessment of personal protective equipment in the post-COVID-19 pandemic. *J. Clean. Prod.* **437**, 140783 (2024).
- Ramalingam, S., Thamizhvel, R., Sudagar, S. & Silambarasan, R. Production of third generation bio-fuel through thermal cracking process by utilizing Covid-19 plastic wastes. *Mater. Today Proc.* **72**, 1618–1623 (2023).
- Demir, A. T. & Moslem, S. Evaluating the effect of the COVID-19 pandemic on medical waste disposal using preference selection index with CRADIS in a fuzzy environment. *Heliyon* **10**, e26997 (2024).
- Masud, R. I. et al. A review on enhanced microplastics derived from biomedical waste during the COVID-19 pandemic with its toxicity, health risks, and biomarkers. *Environ. Res.* **216**, 114434 (2023).
- Dadwal, T., Kumar, V. & Bhatia, U. Experimental investigation on the use of COVID-19 waste in bituminous concrete. *Mater. Today Proc.* **74**, 218–224 (2021).
- Chowdhury, T. et al. Estimation of the healthcare waste generation during COVID-19 pandemic in Bangladesh. *Sci. Total Environ.* **811**, 152295 (2022).
- Neves, R. A. F., Seixas, J. T. C., Rodrigues, N. & Santos, L. N. Impacts of the COVID-19 pandemic restrictions on solid waste pollution in the worldwide iconic Copacabana Beach (Rio de Janeiro, Brazil). *Mar. Pollut. Bull.* **181** (2022).
- Benson, N. U., Basse, D. E. & Palanisami, T. COVID pollution: Impact of COVID-19 pandemic on global plastic waste footprint. *Heliyon* **7**, e06343 (2021).
- Zhang, Q. et al. COVID-19 estimated to have increased plastics, diclofenac, and triclosan pollution in more than half of urban rivers worldwide. *Cell Rep. Sustain.* **1**, 100001 (2024).
- Doad, R., Gupta, R. & Shitak, R. Evaluation of biomedical waste generation in Himachal Pradesh before and during the Covid 19 pandemic. *Sci. Total Environ.* **906**, 167689 (2024).
- Huang, W. et al. Risk evaluation of venue types and human behaviors of COVID-19 outbreaks in public indoor environments: A systematic review and meta-analysis. *Environ. Pollut.* **341**, 122970 (2024).
- Kathiravan, K. et al. Chorographic assessment on the overburden of single-use plastics bio-medical wastes risks and management during COVID-19 pandemic in India. *Total Environ. Res. Themes* **7**, 100062 (2023).
- Saxena, P., Pradhan, I. P. & Kumar, D. Redefining bio medical waste management during COVID-19 in india: A way forward. *Mater. Today Proc.* **60**, 849–858 (2022).
- Ilyas, S., Srivastava, R. R. & Kim, H. Disinfection technology and strategies for COVID-19 hospital and bio-medical waste management. *Sci. Total Environ.* **749**, 141652 (2020).
- Alomari, A. H., Aga, O., El Sahmarany, L., Hegazi, M. & Almulla, L. Public perception towards medical waste generated in the environment during the COVID-19 pandemic in Eastern Province. *Saudi Arabia. Heliyon* **7**, e08363 (2021).
- Mohana, A. A. et al. Generation and consequence of nano/microplastics from medical waste and household plastic during the COVID-19 pandemic. *Chemosphere* **311**, 137014 (2023).
- De-la-Torre, G. E. et al. Release of phthalate esters (PAEs) and microplastics (MPs) from face masks and gloves during the COVID-19 pandemic. *Environ. Res.* **215** (2022).
- Katerusha, D. Attitude towards sustainability, study contents and the use of recycled concrete in building construction: Case study Germany and Switzerland. *J. Clean. Prod.* **289**, 125688 (2021).
- Nanayakkara, O. et al. Alkali activated slag concrete incorporating recycled aggregate concrete: Long term performance and sustainability aspect. *Constr. Build. Mater.* **271**, 121512 (2021).
- Liu, Z., Chin, C. S., Xia, J., Lu, J. & Wang, X. Exploring the sustainability of concrete with fly ash, recycled coarse aggregate and biomaterialisation method by life cycle assessment. *J. Clean. Prod.* **406**, 137077 (2023).
- Coffetti, D. et al. Pathways towards sustainable concrete. *Cem. Concr. Res.* **154**, 106718 (2022).
- Liu, F., Zheng, W., Li, L., Feng, W. & Ning, G. Mechanical and fatigue performance of rubber concrete. *Constr. Build. Mater.* **47**, 711–719 (2013).
- He, L. et al. Research on the properties of rubber concrete containing surface-modified rubber powders. *J. Build. Eng.* **35** (2021).
- Gupta, T., Siddique, S., Sharma, R. K. & Chaudhary, S. Investigating mechanical properties and durability of concrete containing recycled rubber ash and fibers. *J. Mater. Cycles Waste Manag.* **23**, 1048–1057 (2021).
- Dong, Q., Huang, B. & Shu, X. Rubber modified concrete improved by chemically active coating and silane coupling agent. *Constr. Build. Mater.* **48**, 116–123 (2013).
- Liu, M., Lu, J., Ming, P. & Yin, Y. Study of fracture properties and post-peak softening process of rubber concrete based on acoustic emission. *Constr. Build. Mater.* **313**, 125487 (2021).
- Su, P., Dai, Q., Li, M., Ma, Y. & Wang, J. Investigation of the mechanical and shrinkage properties of plastic-rubber compound modified cement mortar with recycled tire steel fiber. *Constr. Build. Mater.* **334**, 127391 (2022).

38. Kumar, R. & Dev, N. Mechanical and microstructural properties of rubberized concrete after surface modification of waste tire rubber crumb. *Arab. J. Sci. Eng.* **47**, 4571–4587 (2022).
39. Chen, A. et al. Analytical evaluation of compressive strength for concrete with rubber fine aggregates and the predictive model. *Constr. Build. Mater.* **345**, 128359 (2022).
40. Chen, J., Zhuang, J., Shen, S. & Dong, S. Experimental investigation on the impact resistance of rubber self-compacting concrete. *Structures* **39**, 691–704 (2022).
41. Feng, W. et al. Compressive behaviour and fragment size distribution model for failure mode prediction of rubber concrete under impact loads. *Constr. Build. Mater.* **273**, 121767 (2021).
42. Ma, Q., Shi, Y., Xu, Z., Ma, D. & Huang, K. Research on a multivariate non-linear regression model of dynamic mechanical properties for the alkali-activated slag mortar with rubber tire crumb. *Case Stud. Constr. Mater.* **17**, e01371 (2022).
43. Zhu, J. et al. Reusing COVID-19 disposable nitrile gloves to improve the mechanical properties of expansive clay subgrade: An innovative medical waste solution. *J. Clean. Prod.* **375**, 134086 (2022).
44. Pham, T. M. et al. Dynamic compressive properties of lightweight rubberized concrete. *Constr. Build. Mater.* **238**, 117705 (2020).
45. Shen, L., Yao, X., Di Luzio, G., Jiang, M. & Han, Y. Mix optimization of hybrid steel and polypropylene fiber-reinforced concrete for anti-thermal spalling. *J. Build. Eng.* **63**, 105409 (2023).

Author contributions

T.R.: Conceptualization, Data curation, Experimental operation, Writing(original draft). J.Y.P: Writing(Review & Editing), Funding acquisition, Data Curation. D.W: Investigation, Validation, Supervision. All authors read and approved the final manuscript.

Declarations

Competing interests

The authors declare no competing interests.

Additional information

Correspondence and requests for materials should be addressed to J.P.

Reprints and permissions information is available at www.nature.com/reprints.

Publisher's note Springer Nature remains neutral with regard to jurisdictional claims in published maps and institutional affiliations.

Open Access This article is licensed under a Creative Commons Attribution-NonCommercial-NoDerivatives 4.0 International License, which permits any non-commercial use, sharing, distribution and reproduction in any medium or format, as long as you give appropriate credit to the original author(s) and the source, provide a link to the Creative Commons licence, and indicate if you modified the licensed material. You do not have permission under this licence to share adapted material derived from this article or parts of it. The images or other third party material in this article are included in the article's Creative Commons licence, unless indicated otherwise in a credit line to the material. If material is not included in the article's Creative Commons licence and your intended use is not permitted by statutory regulation or exceeds the permitted use, you will need to obtain permission directly from the copyright holder. To view a copy of this licence, visit <http://creativecommons.org/licenses/by-nc-nd/4.0/>.

© The Author(s) 2024